INTERNATIONAL JOURNAL FOR NUMERICAL METHODS IN FLUIDS
Int. J. Numer. Meth. Fluids 2009; **60**:1103–1126
Published online 24 September 2008 in Wiley InterScience (www.interscience.wiley.com). DOI: 10.1002/fld.1923

Stabilized finite element formulation for incompressible flow on distorted meshes

Ch. Förster[1], W. A. Wall[1,*,†] and E. Ramm[2]

[1]*Chair of Computational Mechanics, Technische Universität München, Boltzmannstraße 15, 85747 Garching, Germany*
[2]*Institute of Structural Mechanics, University of Stuttgart Pfaffenwaldring 7, 70550 Stuttgart, Germany*

SUMMARY

Flow computations frequently require unfavourably meshes, as for example highly stretched elements in regions of boundary layers or distorted elements in deforming arbitrary Lagrangian Eulerian meshes. Thus, the performance of a flow solver on such meshes is of great interest. The behaviour of finite elements with residual-based stabilization for incompressible Newtonian flow on distorted meshes is considered here.

We investigate the influence of the stabilization terms on the results obtained on distorted meshes by a number of numerical studies. The effect of different element length definitions within the elemental stabilization parameter is considered. Further, different variants of residual-based stabilization are compared indicating that dropping the second derivatives from the stabilization operator, i.e. using a streamline upwind Petrov–Galerkin type of formulation yields better results in a variety of cases. A comparison of the performance of linear and quadratic elements reveals further that the inconsistency of linear elements equipped with residual-based stabilization introduces significant errors on distorted meshes, while quadratic elements are almost unaffected by moderate mesh distortion. Copyright © 2008 John Wiley & Sons, Ltd.

Received 11 November 2007; Revised 12 August 2008; Accepted 12 August 2008

KEY WORDS: stabilized finite elements; incompressible flow; distorted meshes; ALE methods; finite element methods; Petrov–Galerkin

1. INTRODUCTION

Residual-based stabilization methods are a common means to simulate incompressible flow problems on Eulerian as well as on deforming grids. In particular, in the latter case, distorted elements are an inherent feature and cannot be avoided.

*Correspondence to: W. A. Wall, Chair of Computational Mechanics, Technische Universität München, Boltzmannstraße 15, 85747 Garching, Germany.
†E-mail: wall@lnm.mw.tum.de

Contract/grant sponsor: German Science Foundation 'Deutsche Forschungsgemeintschaft' Project SFB 404

The effect of element distortion on the error obtained on distorted meshes can hardly be investigated theoretically. An attempt to do so is made here by showing that the presence or the sign of the viscous term within the stabilization operator can have a significant impact on the performance of stabilized methods on deformed grids. It turns out that a Galerkin-least-squares (GLS) type of formulation is much more robust than one derived from virtual bubbles (also termed unusual stabilized finite element method, USFEM), while the two differ only in the sign of the second derivatives in the stabilization operator. In contrast to a GLS stabilization, USFEM relies on the correct choice of the element parameter m_k, which is defined by an inverse estimate. However, on distorted meshes (in particular on deforming meshes), this parameter is time dependent and reduces with increasing element distortion. As a consequence, USFEM may lose stability if a constant m_k is employed, which is frequently the case.

The behaviour of stabilization parameters for differently shaped 2D elements has been investigated by Tezduyar and Osawa in [1], where different parameters for various flow directions are compared. A comparative investigation has also been reported by Akin and Tezduyar in [2]. In this later study not only the stabilization parameters, but also solution accuracies are compared for test cases at the advective limit.

The actual sensitivity of residual-based stabilized methods to mesh distortion has to be investigated numerically. The shape of the element may also influence a second key parameter in stabilized schemes: the characteristic element length h_k. We compare seven different definitions of the element length among which are ones defined by Codina and Soto [3], the one given by Taylor *et al.* [4], the one specified by Whiting and Jansen [5] and definitions introduced by Mittal in [6].

As a basic test case, the Kim–Moin flow is used, which allows a comparison with analytical results. Particular emphasize is put on a comparison of linear and quadratic elements as the first suffer from an inherent inconsistency when stabilized by the residual-based stabilization methods. It turns out that the inconsistency deficiency increases with increasing element distortion, which can be understood as a strong argument for higher-order elements. The effect of misplaced edge and centre nodes of quadratic elements are considered separately.

We also repeat a number of calculations performed by Mittal [6] to investigate the influence of highly stretched (high aspect ratio) elements. Here, as in other test cases, quadratic elements perform better in terms of accuracy and show very insensitive with respect to the element length definition used within the stabilization parameter τ_{Mk}. In contrast to the results reported in [6] we do not obtain any instability or oscillations.

After stating the governing equations and the discretization in Section 2, we introduce the stabilized formulation employed in Section 3. Within this section, we also discuss the different element length definitions we wish to compare. Section 4 contains a number of numerical studies of the influence of elemental distortion on the overall result. Conclusions are drawn in Section 5.

2. GOVERNING EQUATIONS AND DISCRETIZATION

The fluid under consideration is assumed as Newtonian and its motion is governed by the incompressible Navier–Stokes equations. Expressed in primitive variables, the vector field of the velocity $\mathbf{u}$ and the scalar field of the pressure p, the flow equations read

$$\mathscr{L}_M(\mathbf{u}, p) = \mathbf{b} \quad \text{in } \Omega \times T \tag{1}$$

$$\mathscr{L}_C \mathbf{u} = 0 \quad \text{in } \Omega \times T \tag{2}$$

DOI: 10.1002/fld

where the operators of linear momentum and continuity are given by

$$\mathscr{L}_M(\mathbf{u}, p) = \left.\frac{\partial \mathbf{u}}{\partial t}\right|_{\mathbf{x}} + \nabla\cdot(\mathbf{u}\otimes\mathbf{u}) - 2\nu\nabla\cdot\boldsymbol{\varepsilon}(\mathbf{u}) + \nabla p \tag{3}$$

$$\mathscr{L}_C\mathbf{u} = \nabla\cdot\mathbf{u} \tag{4}$$

respectively. We use bold symbols to distinguish vector or tensor-valued functions from scalars.

The bounded region Ω in $\mathbb{R}^m$, $m=2,3$ having sufficiently smooth boundary Γ is assumed to be constant in time. The boundary can be decomposed into Γ_N and Γ_D carrying Neumann and Dirichlet boundary conditions, respectively. The Eulerian frame of reference is denoted by $\mathbf{x}$.

Equation (1) has been normalized by the fluid density ρ, thus $\nu=\mu/\rho$ represents the kinematic viscosity and $p=\overline{p}/\rho$ the kinematic pressure, where $\overline{p}$ denotes the physical pressure value. The specific volume force is given by $\mathbf{b}$. The second-order tensor $\boldsymbol{\varepsilon}(\mathbf{u})$ represents the strain rate and depends linearly on the velocity according to

$$\boldsymbol{\varepsilon}(\mathbf{u}) = \tfrac{1}{2}(\nabla\mathbf{u} + (\nabla\mathbf{u})^{\mathrm{T}})$$

The operator of linear momentum (3) is stated in Eulerian description for the clarity of presentation, while stabilized finite elements are used for flows on deforming domains (i.e. arbitrary Lagrangian Eulerian (ALE) formulations) in an equal manner.

2.1. Discretization in time

To discretize the system of equations (1) and (2) in time, the second-order accurate backward differencing (BDF2) scheme is employed which on a general first-order differential equation $\dot{y}=f(y,t)$ reads

$$\frac{y^{n+1}-y^n}{\Delta t} = \frac{1}{3}\frac{y^n-y^{n-1}}{\Delta t} + \frac{2}{3}f(y^{n+1}, t^{n+1}) \tag{5}$$

Applying (5) to the strong form (1) yields

$$\mathbf{u}^{n+1} + \tfrac{2}{3}\Delta t[\mathbf{u}^{n+1}\cdot\nabla\mathbf{u}^{n+1} - 2\nu\nabla\cdot\boldsymbol{\varepsilon}(\mathbf{u}^{n+1}) + \nabla p^{n+1}] = \mathbf{r}^{n+1} \tag{6}$$

where the vector $\mathbf{r}^{n+1}$ contains the right-hand side contributions emerging from the time discretization and the body force vector $\mathbf{b}$ as

$$\mathbf{r}^{n+1} = \tfrac{2}{3}\Delta t\mathbf{b}^{n+1} + \tfrac{4}{3}\mathbf{u}^n - \tfrac{1}{3}\mathbf{u}^{n-1}$$

Performing the temporal discretization prior to the discretization in space reveals the correct operator to be stabilized. This might be of particular concern in the context of very small time steps that yield a dominating zeroth-order term [7].

2.2. Discretization in space

The temporally discretized equation (6) is now discretized in space by means of finite elements. In the usual way the domain Ω is divided into non-overlapping patches, the elements.

To define the Galerkin weak form, we select C^0 Lagrangian finite element spaces $\mathbf{V}^h\subset\mathbf{H}^1(\Omega)$ and $\mathbf{V}_0^h\subset\mathbf{H}_0^1(\Omega)$, where the functions in $\mathbf{V}^h$ satisfy the Dirichlet boundary conditions of the problem,

DOI: 10.1002/fld

while all functions in $\mathbf{V}_0^h$ are zero on Γ_D. The pressure is taken from the space $P^h \subset L_0^2(\Omega)$ of square integrable functions with vanishing mean to account for the free additive constant of the pressure variable.

The discrete variational statement is as follows: seek $\mathbf{u} \in \mathbf{V}^h,\ p \in P^h$ such that

$$B_{\text{gal}}(\{\mathbf{u}, p\}, \{\mathbf{v}, q\}) = (\mathbf{r}, \mathbf{v}) + (\mathbf{h}^{n+1}, \mathbf{v})_{\Gamma_N} \quad \text{for all } (\mathbf{v}, q) \in (\mathbf{V}_0^h, P^h) \tag{7}$$

where the discrete operator $B(\{\mathbf{u}, p\}, \{\mathbf{v}, q\})$ is given by

$$\begin{aligned} B_{\text{gal}}(\{\mathbf{u}, p\}, \{\mathbf{v}, q\}) = (\mathbf{u}, \mathbf{v}) + (\tfrac{2}{3}\Delta t \mathbf{u} \cdot \nabla \mathbf{u}, \mathbf{v}) + (\tfrac{2}{3}\Delta t 2\nu \boldsymbol{\varepsilon}(\mathbf{u}), \boldsymbol{\varepsilon}(\mathbf{v})) \\ -(\tfrac{2}{3}\Delta t p, \nabla \cdot \mathbf{v}) - \beta(\tfrac{2}{3}\Delta t q, \nabla \cdot \mathbf{u}) \end{aligned} \tag{8}$$

Here, $(\cdot, \cdot)$ denotes the L^2 inner product on Ω if not indicated otherwise and $\mathbf{h}^{n+1}$ represents Neumann boundary forces at the time instant $t = t^{n+1}$.

The parameter β in (8) can take the values $\{-1, 1\}$, i.e. it carries the sign of the pressure test function q. Introduced by Barth *et al.* [8], it helps to offer a systematic distinction between related but different residual-based stabilization methods.

Remark

The last term of the Galerkin form (8) originates from the continuity equation (2). Since this equation does not contain time derivatives, the 'time factor' $\frac{2}{3}\Delta t$ in the last term of (8) does not emerge from time discretization, but appears useful in order to serve pressure symmetry.

3. STABILIZED FLUID FORMULATION

It is a well known matter of fact that the Galerkin form (7) is ill posed due to the inf–sup condition in the case of finite elements with equal polynomial order in $\mathbf{V}^h$ and P^h defined on the same triangulation. To stabilize the artificial pressure modes as well as oscillations due to convection, residual-based stabilization is applied.

The stabilized variational problem is given by: find $\mathbf{u} \in \mathbf{V}^h,\ p \in P^h$ such that

$$\begin{aligned} &B_{\text{gal}}(\{\mathbf{u}, p\}, \{\mathbf{v}, q\}) - \sum_k \tau_{Mk}(\mathscr{R}_M(\mathbf{u}, p), \mathscr{L}_M^{\text{stab}}(\mathbf{u}, \{\mathbf{v}, q\}))_k + \sum_k \tau_{Ck}(\mathscr{R}_C(\mathbf{u}), \mathscr{L}_C(\mathbf{v}))_k \\ &\quad = (\mathbf{r}, \mathbf{v}) + (\mathbf{h}^{n+1}, \mathbf{v})_{\Gamma_N} \quad \text{for all } (\mathbf{v}, q) \in (\mathbf{V}_0^h, P^h) \end{aligned} \tag{9}$$

where k counts all elements of the triangulation. The inner products within the stabilization terms indicated by the subscript k have to be evaluated on the element interiors only.

Stabilization with the residual of the continuity equation $\mathscr{R}_C(\mathbf{u})$ has been introduced by Franca and Hughes [9] and offers benefit especially for high Reynolds numbers [10, 11]. Franca and Oliveira [12] also showed that the continuity stabilization term can, similar to the momentum one, be recovered as static condensation of a bubble function.

The stabilization is based on the temporally discretized residuals

$$\mathscr{R}_M(\mathbf{u}^{n+1}, p^{n+1}) = \mathbf{u}^{n+1} + \tfrac{2}{3}\Delta t[\mathbf{u}^{n+1} \cdot \nabla \mathbf{u}^{n+1} - 2\nu \nabla \cdot \boldsymbol{\varepsilon}(\mathbf{u}^{n+1}) + \nabla p^{n+1}] - \mathbf{r}^{n+1} \tag{10}$$

$$\mathscr{R}_C(\mathbf{u}^{n+1}) = \nabla \cdot \mathbf{u}^{n+1} \tag{11}$$

DOI: 10.1002/fld

and employs the stabilization operators

$$\mathscr{L}_M^{\text{stab}}(\mathbf{u}, \{\mathbf{v}, q\}) = \eta\mathbf{v} + \tfrac{2}{3}\Delta t\,(-\mathbf{u}\cdot\nabla\mathbf{v} - \alpha 2\nu\nabla\cdot\boldsymbol{\varepsilon}(\mathbf{v}) + \beta\nabla q) \tag{12}$$

$$\mathscr{L}_C^{\text{stab}}(\mathbf{v}) = \mathscr{L}_C(\mathbf{v}) = \nabla\cdot\mathbf{v} \tag{13}$$

A number of related stabilization methods are specified by different parameter combinations of $\eta\in\{0,1\}$, $\alpha\in\{-1,0,1\}$ and β. All the possible methods are consistent in the sense that sufficiently smooth solutions of the strong equations (1) and (2) satisfy the stabilized discrete form (9). Using $\eta=1$, $\alpha=1$ and $\beta=-1$, i.e. employing the adjoint of the linearized operator yields the unusual stabilized method of Franca and coworkers [13–15]. Setting $\eta=0$, $\alpha=-1$ and $\beta=-1$ reveal the GLS stabilization for the corresponding stationary operator. Using $\alpha=0$, i.e. dropping the viscous term from the stabilization operator yields a method in the sense of the streamline upwind Petrov–Galerkin (SUPG) stabilization. An overview over properties of different schemes (in terms of α and β) in the case of the stationary Stokes problem has been given in [8]. It can be shown that the use of a zeroth-order term within the stabilization operator offers some benefit in the context of dominating zeroth-order terms, while it should not be used in conjunction with linear elements in space [16].

The stabilization parameters used are the one developed from virtual bubble functions for the linear Stokes problem [17] or the reaction–advection–diffusion equation [15], to stabilize the mixed problem or the advective term, respectively. The parameters have been adopted to the formulation used here.

$$\tau_{Mk} = \frac{h_k^2}{h_k^2\xi_1 + \dfrac{8\Delta t\,\nu}{3m_k}\xi_2} \tag{14}$$

The parameters ξ_1 and ξ_2 depend on the effects dominating the flow in a particular element

$$\xi_1 = \max(r_k, 1), \quad \xi_2 = \max(Re_k, 1)$$

where Re_k is a measure of an elemental Reynolds number and represents the ratio of advective to viscous forces on element level. The symbol r_k denotes the ratio of the viscous, second-order term to the zeroth-order term introduced by time integration

$$r_k = \frac{8\Delta t\,\nu}{3m_k h_k^2}$$

$$Re_k = \frac{m_k|\mathbf{u}|h_k}{2\nu}$$

The Euclidean norm of the velocity $|\mathbf{u}|$ is used here as a measure of the convective term, where the parameter

$$m_k = \min\{\tfrac{1}{3}, C_k\} \tag{15}$$

carries the influence of the particular discretization. It is defined by an inverse estimate [15, 18] while here a local definition is employed

$$C_k h_k^2 \|\Delta\mathbf{v}\|_k^2 \leqslant \|\nabla\mathbf{v}\|_k^2 \quad \text{for all } \mathbf{v}\in\mathbf{V}_k^h \tag{16}$$

DOI: 10.1002/fld

where $\mathbf{V}_k^h$ is the restriction of the discrete space $\mathbf{V}^h$ on the element k. Based on the analysis given in [18], $m_k = \frac{1}{3}$ and $m_k = \frac{1}{12}$ are used for linear and quadratic elements, respectively. The significance of m_k will be discussed further in Section 4.

Employing the above definitions, the continuity stabilization parameter is given by

$$\tau_{Ck} = \frac{2\Delta t h_k |\mathbf{u}|}{6} \xi_2$$

This parameter is of particular interest in the high Reynolds number regime and thus given here for completeness only.

3.1. Inconsistency of linear elements

The discrete Galerkin weak form stems from a weighted residual of the temporally discretized equation (6), which is enhanced by adding the residual element wise weighted by the stabilization operator. Let us assume sufficient smoothness of the velocity approximation and consider the weighted residual method including stabilization terms read

$$(\mathscr{R}_M, \mathbf{v}) + (\mathscr{R}_C, q) - \sum_k \tau_{Mk} (\mathscr{R}_M, \mathscr{L}_M^{\text{stab}})_k + \sum_k \tau_{Ck} (\mathscr{R}_C, \mathscr{L}_C)_k = 0 \tag{17}$$

The stabilized form (9) is obtained from (17) by integrating the stress term within the first terms by parts, which reduces the continuity requirement for the velocity to standard C^0 continuity. No such modification is done on the stabilization part. Thus, within the stabilization terms, the residual of the linear momentum equation $\mathscr{R}_M$ contains second derivatives which cannot be represented correctly by linear elements. Suggestions to avoid or at least reduce this inconsistency for low-order elements have been made by Jansen and coworkers [19], while the proposed modifications belong to the class of variational crimes and do not show a significant improvement on the distorted meshes considered here. In [1], Tezduyar and Osawa suggest to introduce the flux jump terms into the stabilized formulation. This approach requires the evaluation of element boundary integrals for all elements.

For purely linear elements, i.e. three-noded triangles in 2D and four-noded tetrahedrons in 3D, the residual of the momentum equation which is used within the stabilization term reduces to

$$\mathscr{R}_{M,\text{lin}}^{\text{stab}} = \mathbf{u}^{n+1} + \tfrac{2}{3}\Delta t [\mathbf{u}^{n+1} \cdot \nabla \mathbf{u}^{n+1} + \nabla p^{n+1}] - \mathbf{r}^{n+1}$$

where for general bi- or trilinear elements a rudiment of the viscous part remains, which is unable to properly represent the respective term but rather deteriorates accuracy.

The incompletely resolved second derivatives are included not only in the residuum, but also within the stabilization operator as soon as USFEM or GLS type of stabilization is employed (i.e. $\alpha \neq 0$). Numerical observations indicate that these derivatives in the weighting term are an additional source of inaccuracy if bilinear or trilinear elements are employed.

As the so introduced consistency error scales with the stabilization parameter τ_{Mk}, it diminishes at spatial or temporal refinement. While not affecting the convergence rates, it is present for particular discretizations with linear elements. Thus, in such simulations a part of the error is to be found, which scales directly with the stabilization parameter. Consequently, it is of particular importance to employ a stabilization parameter as small as possible when linear elements are used in conjunction with residual-based stabilization methods. A lower bound on the stabilization parameter is required to prevent the artificial pressure modes resulting from the violation of the inf–sup condition.

DOI: 10.1002/fld

3.2. Element length definitions

The characteristic element length h_k has a significant impact on the actual amount of stabilization employed as at the viscous limit the stabilization parameter is proportional to h_k^2 while it is linear in h_k at the convective limit. Especially, in the context of mesh distortion or highly elongated elements, the element length definition has to be chosen carefully [6].

Various definitions have been suggested and discussed in the literature. An overview can be found in [11], where also the suggestion was made to use different element lengths within the different terms. A geometric 'isotropic' element length definition (for example, the square root of the elemental area) is suggested when the viscous terms dominate, while a streamlength is used for convection-dominated flows. Within this paper the following definitions for the characteristic element lengths are compared by numerical investigations

(i) square root of element area,

$$h_k = \sqrt{A_k}$$

(ii) element length in flow direction [11] evaluated once at element centre,

(iii) approximate element length in flow direction as defined by Codina and Soto in [3]

$$h_k = \frac{|\mathbf{u}|}{|\mathbf{u}_0|} h_0$$

where the subscript 0 refers to the reference configuration, and

(iv) element length for anisotropic meshes as defined by Codina and Soto in [3], where the smallest eigenvalue of the operator $\mathbf{B}$ is taken as a characteristic element length. $\mathbf{B}$ stems from the polar decomposition of the Jacobian $\mathbf{J}$ of the isoparametric mapping to the element domain, i.e. $\mathbf{J} = \mathbf{BZ}$, where $\mathbf{B}$ is symmetric and positive-definite, whereas $\mathbf{Z}$ is orthogonal.

Further an implicit definition of the element length which has been suggested by Taylor, Hughes and coworkers [4, 5] is also included into the comparison.

(v) Employing the covariant coordinates of the metric tensor g_{ij} of the mapping from global Cartesian coordinates to the element parameters, the stabilization parameter is given by

$$\tau_{\mathrm{M}e} = (4 + \tfrac{4}{9}(\Delta t)^2 (u_i g_{ij} u_j + c v^2 g_{ij} g_{ij}))^{-1/2}$$

where the constant c is set to 36 and to 60 for linear and quadratic elements, respectively [5, 20]. The corresponding stabilization parameter for the continuum equation is given by

$$\tau_{\mathrm{C}e} = (8 \tau_{\mathrm{M}e} \operatorname{tr}(g_{ij}))^{-1}$$

Additionally, the element length definitions investigated by Mittal [6] are considered as parts of the computations reported in [6] are repeated here.

(vi) minimal element length given by

$$h_k = h_{k,\min} = \frac{\sqrt{2} A_e}{\max(h_{\mathrm{diag}})} \tag{18}$$

DOI: 10.1002/fld

(vii) maximal element length defined as the edge length of a square with a diagonal of $\max(h_{\text{diag}})$

$$h_k = h_{k,\max} = \frac{\max(h_{\text{diag}})}{\sqrt{2}} \tag{19}$$

Although the element length definitions (i), (iv) and (v) to (vii) are purely geometrical, the streamlength (ii) and (iii) depends upon the velocity and hence adds to the overall nonlinearity. Consequently, the convergence rate of the fluid iterations decreases when these stabilization parameters are employed. In complex situations convergence may even be lost. In order to fix this problem, linearization of the stabilization parameter with respect to the velocity could be performed. Numerical investigations indicate that streamlength computation is not essential and geometrical definitions of the characteristic element length may work equally well.

In [1, 21], Tezduyar and Osawa suggest to circumvent the nonlinearity by defining stabilization parameters based on the solution of the previous time step.

The list of element length definitions is by far not complete. There is a number of alternative definitions that can be found in the literature among which is the so-called 'advective length scale' introduced in [22]. Another example also suggested by Tezduyar is the so-called 'diffusive length scale' introduced in [21]. Both length scale definitions behave very similar to the ones investigated subsequently, whereas both depend upon the unknown velocity and add to the overall nonlinearity.

4. DISTORTED MESHES

The sensitivity of stabilized methods with respect to distorted and unfavourably shaped elements is hard to access analytically. Numerical tests have to be performed since. However, a systematic failure of the USFEM stabilization variant with fixed parameter m_k at a particular amount of mesh distortion can be explained by the properties of the respective stabilization terms.

4.1. Sensitivity of USFEM stabilization variant

4.1.1. Influence of m_k. Numerical investigations reveal that the USFEM implementation with $\alpha = 1$ and $m_k = \frac{1}{12}$ becomes unstable at a certain level of mesh distortion. The observed instability is caused by a stabilization term and can easily be shown at the model problem of an unusual stabilized diffusion problem given by: find $\varphi \in \mathbf{V}^h$ such that

$$(\nabla\varphi, \nabla v) - \sum_k (\Delta\varphi, \tau_k \Delta v)_k = (b, v) - \sum_k (b, \tau_k \Delta v)_k \quad \text{for all } v \in \mathbf{V}_0^h \tag{20}$$

Equation (20) represents an unusual stabilized formulation of the Laplace equation $-\Delta\varphi = b$ and defines a bilinear form $B(\varphi, v)$ the coercivity of which depends upon the proper choice of the stabilization parameter τ_k.

$$B(\varphi, \varphi) = \|\nabla\varphi\|^2 - \sum_k \tau_k \|\Delta\varphi\|_k^2$$

Employing the inverse inequality that is also used for the definition of m_k (16), we obtain

$$B(\varphi, \varphi) \geqslant \sum_k \left(1 - \frac{\tau_k}{C_k h_k^2}\right) \|\nabla\varphi\|_k^2$$

DOI: 10.1002/fld

yielding the condition

$$\tau_k < C_k h_k^2 \tag{21}$$

In the viscous limit (and with a unit kinematic viscosity), the stabilization parameter given by the definition (14) reduces to

$$\tau_k = \frac{h_k^2 m_k}{4}$$

which together with (21) yields the stability condition

$$m_k < 4C_k \tag{22}$$

The condition (22) is satisfied when the correct definition of m_k is used. Thus, for a proper use of the unusual stabilized method on distorted meshes, it proves essential to employ the correct definition of the parameter m_k (16) rather than working with a fixed constant as it is frequently reported in the literature.

The parameter m_k enters the stabilization parameter in order to account for the ratio of the first and second derivatives in the finite element space. Element distortion highly influences this ratio and thus demands an accurately determined parameter m_k. Owing to the local nature of the inverse estimate (16), the constant C_k is an elemental geometry parameter and can be obtained locally. However, a correct determination of the constant C_k requires the solution of the eigenvalue problem inherent in (16) for every element once per time step if the mesh moves significantly during the computation. While being correct, such a procedure is too much expensive for practical applications.

The above derivation shows that the potential instability occurs since an USFEM used on an operator that contains a Laplace term, yields a subtraction of a term containing second derivatives with a potentially destabilizing effect. However, this term can be removed by employing a SUPG method rather than USFEM, i.e. by setting $\alpha = 0$ within the stabilization operator (12). Using $\alpha = 1$ changes the sign of the respective terms and hence adds stabilization rather than subtracting it. In the latter case, the GLS is recovered. The unconditional stability of the stabilized method obtained by setting $\alpha = 1$ has already been noticed by Douglas and Wang in 1989 [23] and is of particular interest in the context of deforming meshes.

4.1.2. Determination of m_k. To determine the constant C_k that exactly satisfies the inverse estimate (16) for a particular element k with given shape results in an eigenvalue problem. Estimates of the constant for a variety of different elements have been provided by Harari and Hughes in [18]. In [24], Franca and Madureira suggest to use a stabilization parameter where the solution of this eigenvalue problem is worked in.

The norms of the gradient and the Laplacean define symmetric positive-definite (or semi-definite) local operator matrices by

$$\|\nabla \mathbf{v}\|_k^2 = \mathbf{v}^{\mathrm{T}} \mathbf{K} \mathbf{v} \quad \text{and} \quad \|\Delta \mathbf{v}\|_k^2 = \mathbf{v}^{\mathrm{T}} \mathbf{L} \mathbf{v}$$

where $\mathbf{v}$ denotes the nodal degrees of freedom with respect to the nodal base of $\mathbf{V}_k^h$. The maximal eigenvalue λ_1 of the generalized eigenvalue problem is

$$\det(\mathbf{K} - \lambda_i \mathbf{L}) = 0$$

yields the sharp constant $C_k = \lambda_1 / h_k^2$.

DOI: 10.1002/fld

As the correct value of the parameter C_k can be crucial in USFEM the solution of one eigenvalue problem per element is required. In the case of an moving ALE mesh, a stable USFEM implementation is obtained only if C_k is determined for every element after each mesh motion step, which makes the algorithm rather expensive and should be avoided.

4.2. Distorted linear and quadratic quadrilaterals

The two-dimensional Kim–Moin flow is one of the rare academic examples for which an analytical solution of the incompressible Navier–Stokes equations is known. The problem shall serve here for a general comparison of all the stabilization parameter definitions listed in Section 3.2.

The Kim–Moin model problem is solved on the unit square $\Omega=[0,1]\times[0,1]$ and compared with its exact solution reading

$$u_x(x,y,t) = -\cos(a\pi x)\sin(a\pi y)\mathrm{e}^{-2a^2\pi^2 tv} \tag{23}$$

$$u_y(x,y,t) = \sin(a\pi x)\cos(a\pi y)\mathrm{e}^{-2a^2\pi^2 tv} \tag{24}$$

$$p(x,y,t) = -\tfrac{1}{4}(\cos(2a\pi x)+\cos(2a\pi y))\mathrm{e}^{-4a^2\pi^2 tv} \tag{25}$$

An impression of the flow field is given in Figure 1 where velocity vectors on the corresponding pressure field are depicted. According to (23)–(25), velocity and pressure field remain in space and decrease monotonically in time.

The solution (23)–(25) is a product of a spatial and a temporal solution, which allows easy scaling of the error in order to remove the temporal decay of the error, which is due to the decay of the solution. Thus, the errors reported are absolute spatial errors defined by

$$\begin{aligned} \mathrm{err}_{\mathbf{u}} &:= \|\mathbf{u}^h - \mathbf{u}\|_0 \mathrm{e}^{2a^2\pi^2 tv} \\ \mathrm{err}_p &:= \|p^h - p\|_0 \mathrm{e}^{4a^2\pi^2 tv} \end{aligned} \tag{26}$$

where the superscript h indicates the numerical solution and $\|\cdot\|_0$ the usual L^2 norm.

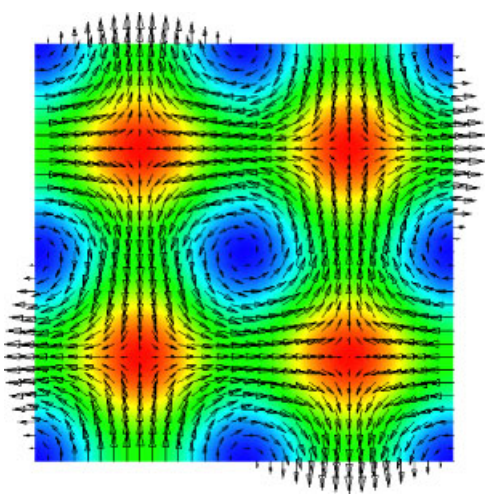

Figure 1. Kim–Moin flow-velocity vectors on pressure field.

DOI: 10.1002/fld

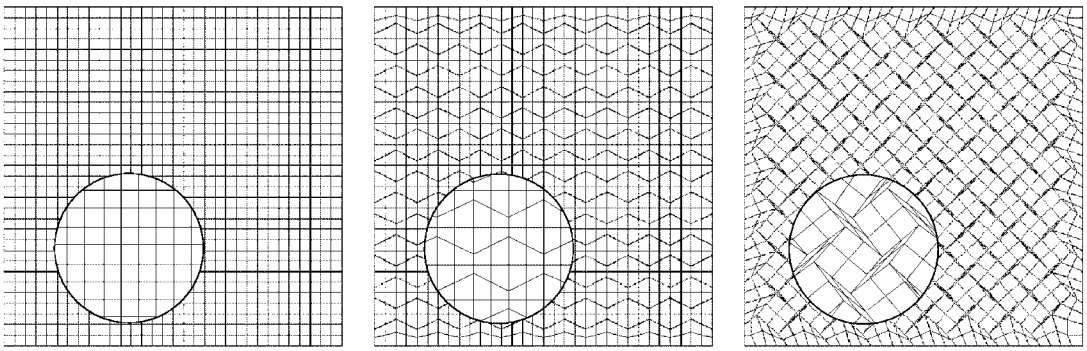

Figure 2. Meshes used for error evaluation with zoom area: (a) undistorted mesh for reference; (b) distortion mode 1; and (c) distortion mode 2.

The calculations reported here have been performed with the parameter $a=2.0$ and a kinematic viscosity of $\nu=0.01$. BDF2 has been used for temporal discretization with a time step size of $\Delta t=0.01$. The errors after 100 time steps are compared in different discretizations and with linear Q1Q1 and quadratic Q2Q2 elements both with equal interpolation order of pressure and velocity. 32×32 and 16×16 elements are used with the linear and quadratic elements, respectively, giving the same number of unknowns in either case.

Within this example no steep gradients occur. Thus, the stabilization methods that are compared are the ones defined by $\eta=0$, $\alpha=-1$, $\beta=-1$ (GLS), and $\eta=\alpha=0$, $\beta=-1$ (SUPG) both with fixed m_k.

Two different distortion modes are investigated as depicted in Figure 2(b) and (c). The first degenerates the quadratic elements to trapezoids, while the second introduces very slender rhombuses, which turned out to appear easily when the mesh moves. The distorted Q2Q2 elements work on the same nodal distributions, i.e. it has perfectly placed edge and centre nodes and straight element edges.

An impression of the error distribution in two examples is given in Figure 3, where the absolute value of the difference of numerical and analytical solution, i.e. $|\mathbf{u}^h-\mathbf{u}|e^{2a^2\pi^2 t\nu}$ is plotted. The figure shows results obtained with linear GLS stabilized elements with stabilization parameter according to definition (i). The error distribution on the undistorted mesh and the mesh in distortion mode 2 are presented. In the latter case, the maximal deviation from the analytical solution is more than 250 times larger than on the regular mesh. However, the error distribution itself appears remarkably similar and closely related to the pattern of the solution. This indicates that in both cases the primary error source is numerical dissipation yielding a faster decay of the flow.

The errors obtained on a regular mesh with equal-sized squared elements as depicted in Figure 2(a) using the two different discretizations and the stabilization parameters introduced in Section 3 are summarized in Table I. These results show that even on meshes of perfectly shaped elements a quadratic interpolation works significantly better than a linear one. This difference is mainly due to the inherent inconsistency of linear elements, which fail to properly approximate second derivatives necessary within the stabilization terms. The errors obtained with SUPG stabilization (i.e. setting α to zero) highlight this effect. While linear elements perform better with SUPG rather than GLS, there is almost no difference when quadratic elements are employed.

DOI: 10.1002/fld

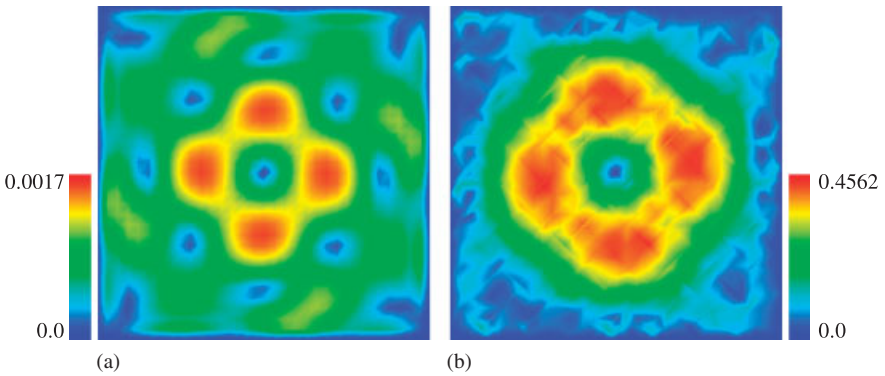

Figure 3. Distribution of absolute value of normalized velocity error obtained with linear elements after 100 time steps: (a) on distortion mode 0 and (b) on distortion mode 2.

Table I. L^2 error in velocity and pressure on undistorted meshes of linear Q1Q1 and quadratic Q2Q2 elements for different choices of stabilization parameter and element length definition.

τ	$\mathrm{err}_{\mathbf{u}}$ Q1Q1 GLS	err_{p} Q1Q1 GLS	$\mathrm{err}_{\mathbf{u}}$ Q1Q1 SUPG	err_{p} Q1Q1 SUPG	$\mathrm{err}_{\mathbf{u}}$ Q2Q2 GLS	err_{p} Q2Q2 GLS	$\mathrm{err}_{\mathbf{u}}$ Q2Q2 SUPG	err_{p} Q2Q2 SUPG
(i)	0.005130	0.002877	0.004614	0.002460	0.002624	0.002560	0.002617	0.002544
(ii)	0.005267	0.002919	0.004729	0.002505	0.002623	0.002562	0.002616	0.002546
(iii)	0.005130	0.002877	0.004614	0.002460	0.002624	0.002560	0.002617	0.002544
(iv)	0.005130	0.002877	0.004614	0.002460	0.002624	0.002560	0.002617	0.002544
(v)	0.004815	0.002885	0.004524	0.002676	0.002631	0.002561	0.002624	0.002546
(vi)	0.005130	0.002877	0.004614	0.002460	0.002624	0.002560	0.002617	0.002544
(vii)	0.005130	0.002877	0.004614	0.002460	0.002624	0.002560	0.002617	0.002544

The results given in Table I also show that the element length definitions (i), (iii), (iv), (vi) and (vii) yield the same result on squared meshes as the element length definitions give equal characteristic lengths in the special case of perfectly squared elements. As soon as element distortion is considered differences occur.

Clearly, the errors related to the second-order terms decrease with decreasing viscosity, i.e. for higher Reynolds numbers the effect will be less important. However, it will always play its role in diffusion dominated areas such as boundary layers. Thus, residual-based stabilization methods at finite Reynolds numbers should be used with the problem of poorly resolved higher-order terms in mind.

The errors obtained on the mesh in distortion mode 1 are summarized in Table II and show an even bigger difference between linear and quadratic elements. On distorted meshes of bilinear elements, the bad representation of second derivatives tends to spoil the results. Employing SUPG stabilization rather than full GLS removes the erroneous second derivatives from the stabilization operator improving the results slightly. The residual itself, however, remains insufficiently represented still causing errors almost twice as big as the ones obtained by quadratic elements, which are hardly affected by the element distortion in mode 1.

DOI: 10.1002/fld

Table II. L^2 error in velocity and pressure on mode 1 distorted meshes of linear Q1Q1 and quadratic Q2Q2 elements for different choices of stabilization parameter and element length definition.

τ	$\mathrm{err}_{\mathbf{u}}$ Q1Q1 GLS	err_p Q1Q1 GLS	$\mathrm{err}_{\mathbf{u}}$ Q1Q1 SUPG	err_p Q1Q1 SUPG	$\mathrm{err}_{\mathbf{u}}$ Q2Q2 GLS	err_p Q2Q2 GLS	$\mathrm{err}_{\mathbf{u}}$ Q2Q2 SUPG	err_p Q2Q2 SUPG
(i)	0.007613	0.005044	0.006514	0.004266	0.002638	0.002581	0.002637	0.002587
(ii)	0.007695	0.004969	0.006593	0.004199	0.002636	0.002581	0.002635	0.002590
(iii)	0.007513	0.004839	0.006460	0.004083	0.002638	0.002580	0.002637	0.002587
(iv)	0.007376	0.004821	0.006444	0.004207	0.002642	0.002583	0.002641	0.002589
(v)	0.006994	0.004825	0.006353	0.004376	0.002648	0.002584	0.002644	0.002588
(vi)	0.007422	0.004913	0.006456	0.004251	0.002642	0.002583	0.002641	0.002589
(vii)	0.007785	0.005177	0.006575	0.004321	0.002635	0.002579	0.002634	0.002586

Table III. L^2 error in velocity and pressure on mode 2 distorted meshes of linear Q1Q1 and quadratic Q2Q2 elements for different choices of stabilization parameter and element length definition.

τ	$\mathrm{err}_{\mathbf{u}}$ Q1Q1 GLS	err_p Q1Q1 GLS	$\mathrm{err}_{\mathbf{u}}$ Q1Q1 SUPG	err_p Q1Q1 SUPG	$\mathrm{err}_{\mathbf{u}}$ Q2Q2 GLS	err_p Q2Q2 GLS	$\mathrm{err}_{\mathbf{u}}$ Q2Q2 SUPG	err_p Q2Q2 SUPG
(i)	0.232357	0.185340	0.043555	0.084645	0.006558	0.009451	0.004198	0.010419
(ii)	0.134009	0.120765	0.055546	0.058709	0.006135	0.008265	0.004601	0.010309
(iii)	0.108969	0.102256	0.057660	0.061274	0.005910	0.008046	0.004624	0.010148
(iv)	0.087337	0.085032	0.058018	0.057737	0.004953	0.007794	0.004212	0.006309
(v)	0.087531	0.087089	0.058085	0.059084	0.005621	0.008779	0.004048	0.004463
(vi)	0.087356	0.085038	0.058027	0.057756	0.004952	0.007793	0.004212	0.006316
(vii)	0.419851	0.272936	0.043516	0.155843	0.006916	0.010307	0.004510	0.018528

Within difficult geometries mesh motion often results in highly stretched arbitrary shapes for elements with extreme angular distortion. The distortion mode 2 has been designed as a test case of such situations. The results summarized in Table III show the devastating effect this element distortion has on linear elements accuracy. Compared with the results obtained with the perfect mesh depicted in Figure 2(a), the errors increase about two orders of magnitude and the result can be regarded as spoilt by these errors. Quadratic elements on the same mesh perform significantly better. An increase of the error has to be expected as the distortion introduces larger elements exhibiting a poorer approximation quality. But while the error of the quadratic elements is doubled or tripled compared with the previous calculations it is still small compared with the solution.

Additionally to the element lengths reported in Tables I–III, also the mentioned advective and diffusive length scale suggested by Tezduyar *et al.* have been tested. Although one might suppose that in particular the diffusive length scale could behave well for the present problem, this is not the case. The errors are in the range spanned by the other parameters. For the diffusive length scale on the mesh 2(c), convergence is even lost.

A graphical representation of the L^2 errors of pressure and velocity is given in the Figures 4 and 5, respectively. It highlights the relative magnitude of the errors on a linear scale and confirms the previous discussion.

The results obtained on distortion mode 1 and 2 show only very little difference between the different stabilization parameters, i.e. element length definitions. When linear elements are

DOI: 10.1002/fld

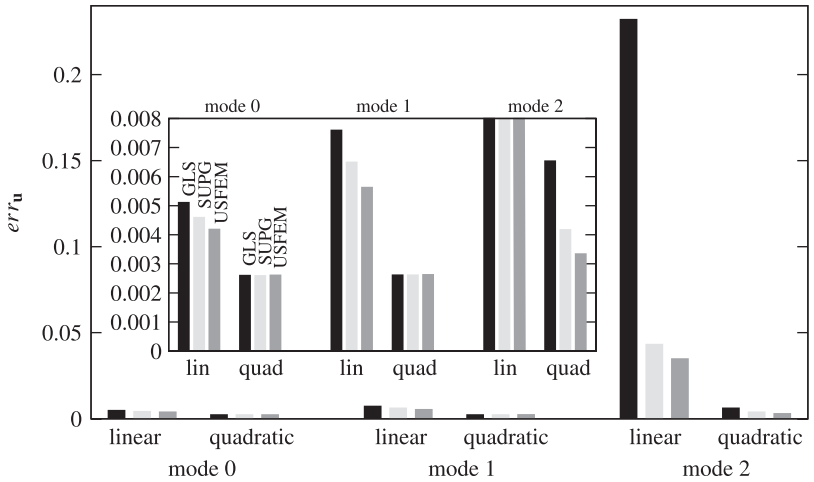

Figure 4. Velocity error obtained on differently distorted meshes with linear and quadratic elements, and GLS, SUPG and USFEM configuration of the stabilization and element length definition (i).

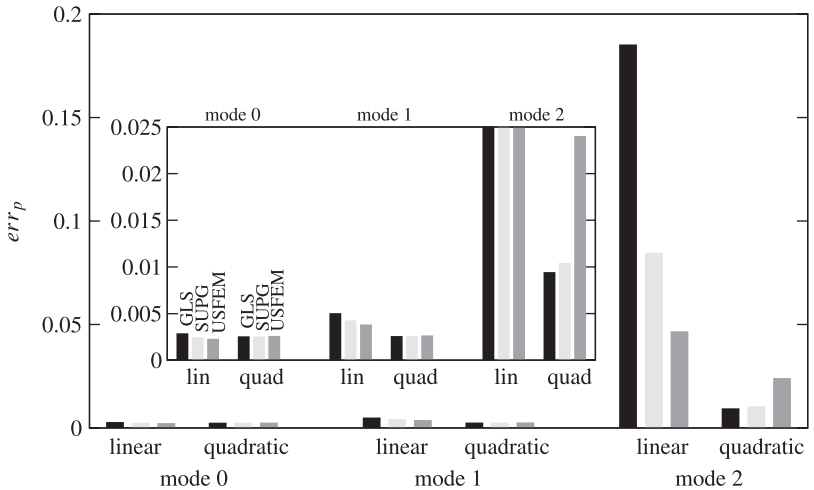

Figure 5. Pressure error obtained on differently distorted meshes with linear and quadratic elements, and GLS, SUPG and USFEM configuration of the stabilization and element length definition (i).

employed the velocity error generally increases with increasing stabilization as the insufficiently resolved residual gets higher influence on the solution. Using SUPG rather than USFEM or GLS with linear elements reduces the error by one order of magnitude, which again blames the badly represented second derivatives for the error. Thus, for computations on distorted meshes higher-order elements are strongly suggested.

However, it is also clearly visible that in all distorted cases large errors are obtained with the stabilization parameter employing the length definition (vii), i.e. using a large characteristic element

DOI: 10.1002/fld

Table IV. Velocity and pressure error in normalized $\mathbf{H}^1$ seminorm on differently distorted meshes of linear Q1Q1 elements.

Mode	$\text{graderr}_{\mathbf{u}}$ Q1Q1 GLS	graderr_p Q1Q1 GLS	$\text{graderr}_{\mathbf{u}}$ Q1Q1 SUPG	graderr_p Q1Q1 SUPG
0	0.357003	0.356385	0.356671	0.356563
1	0.455323	0.448726	0.432784	0.431555
2	2.894864	7.005269	2.049585	15.375787

Table V. Velocity and pressure error in normalized $\mathbf{H}^1$ seminorm on differently distorted meshes of quadratic Q2Q2 elements.

Mode	$\text{graderr}_{\mathbf{u}}$ Q2Q2 GLS	graderr_p Q2Q2 GLS	$\text{graderr}_{\mathbf{u}}$ Q2Q2 SUPG	graderr_p Q2Q2 SUPG
0	0.042845	0.082813	0.043054	0.083754
1	0.059931	0.109139	0.058817	0.110863
2	0.405593	0.912929	0.281089	2.893050

length. Thus, care has to be taken to avoid over-stabilization that yields particularly devastating results in conjunction with linear elements.

The superiority of quadratic elements is confirmed if the gradient errors are considered. In accordance with (26) a normalized $\mathbf{H}^1$ seminorm of the error can be defined, which is independent of the temporal decay

$$\begin{aligned} \text{graderr}_{\mathbf{u}} &:= \|\nabla \mathbf{u}^h - \nabla \mathbf{u}\|_0 \mathrm{e}^{2a^2\pi^2 t\nu} \\ \text{graderr}_p &:= \|\nabla p^h - \nabla p\|_0 \mathrm{e}^{4a^2\pi^2 t\nu} \end{aligned} \tag{27}$$

The $\mathbf{H}^1$ seminorm of the error is calculated with the element length definition (i), and for the three different modes of mesh distortion are given in the Tables IV and V. These errors confirm the previous observations and show a particular sensitivity of the pressure gradient with respect to mesh distortion. Interestingly, this sensitivity even increases when the SUPG version of the stabilization is employed.

4.3. Quadratic elements with misplaced edge and centre nodes

There is a large number of possible distortion modes for quadratic and higher-order elements by displacement of edge and surface nodes. Misplaced edge and centre nodes can have a huge impact on the accuracy obtained by the higher-order elements. However, usually there is no need for allowing arbitrary placement of the non-corner nodes in the elements inside the domain. Only at curved boundaries edge nodes of higher-order elements have to be placed outside the straight line defined by the two adjacent corner points.

Nevertheless, we investigate the effect of misplaced edge nodes in the interior of the domain as we wish to experience the error sensitivity due to such displacements. Our investigation is restricted

DOI: 10.1002/fld

to the edge nodes displaced perpendicular to the undistorted element edge while still residing on the centre of the new curved edge. The element mid nodes are placed in the centres of the distorted elements.

The Kim–Moin flow problem discretized by 16×16 Q2Q2 elements is used again as a test case. The parameters are the same ones as before and again we compare the time-normalized error after 100 steps of $\Delta t = 0.01$. The distorted meshes under consideration are depicted in Figure 6 where the offset of the edge node perpendicular to the undistorted element edge d is varied between $0 \leqslant d \leqslant 1.5h$, where h denotes the distance between two adjacent nodes in the original mesh, i.e. half the original element length.

We use the element length defined in point (i) for the computation of the errors according to (26). The diagrams in Figure 7 show the evolution of the normalized velocity and pressure error when the amount of distortion d is changed.

From the diagrams in Figure 7, it can be seen that small or moderate displacements of the edge node perpendicular to the straight edge can be done without introducing the velocity or pressure errors due to mesh distortion. Huge displacements of the edge node yield clear deterioration of

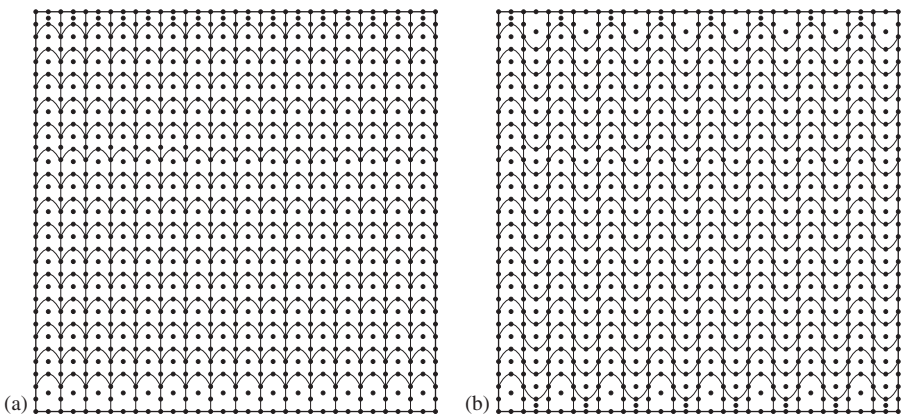

Figure 6. Distorted Q2Q2 element meshes with displayed edge nodes at $d = h$: (a) distortion mode 3 and (b) distortion mode 4.

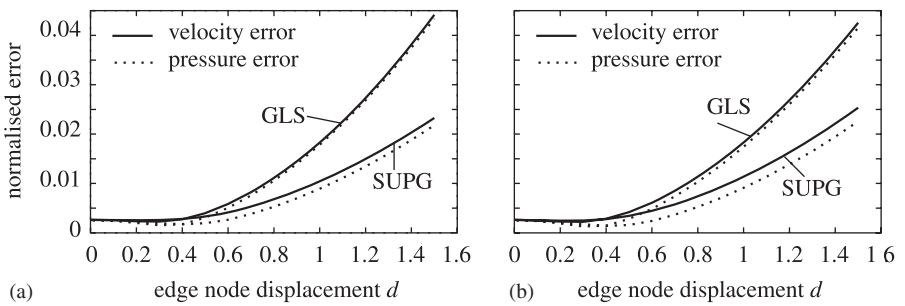

Figure 7. Evolution of the normalized error depending upon the distortion d of the edge nodes in distortion: (a) mode 3 and (b) mode 4.

DOI: 10.1002/fld

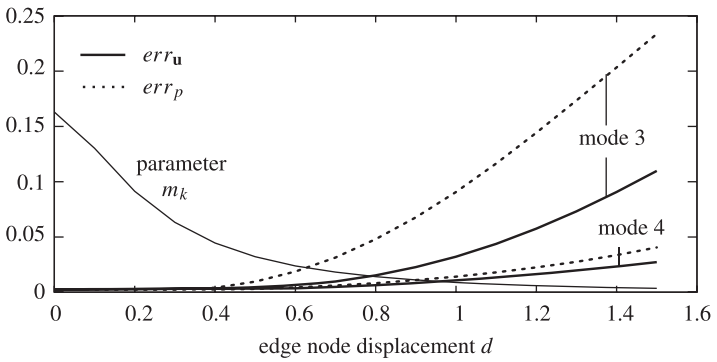

Figure 8. Evolution of the normalized error obtained with USFEM stabilization for distortion modes 3 and 4 along with the parameter m_k.

the results. It is further observed that the SUPG type of the stabilization method, i.e. $\alpha=0$ yields significantly smaller errors in velocity and pressure than GLS when high edge node offsets are considered. Badly approximated second derivatives are able to affect quadratic elements also if high distortion has to be considered. In most practical cases, however, good geometry approximation should be possible by placing the edge node with $-0.5h\leqslant d\leqslant 0.5h$, i.e. with an offset of up to a quarter of the element length.

A different behaviour is observed if a USFEM version of the stabilization is employed, i.e. if $\alpha=1$ (where still $\eta=0$ is used). In this case an elemental constant m_k is determined according to (15) has to be employed. The errors obtained on the two meshes depicted in Figure 6 are displayed in Figure 8 along with the evolution of the parameter m_k.

The diagram in Figure 8 shows that the errors obtained for USFEM and the distortion mode 3 are much larger than those of all other cases. Additionally, the pressure error here significantly exceeds the corresponding velocity error. This effect is due to the necessary drop in the parameter m_k. Along with a reduced m_k, the stabilization parameter $\tau_{\mathrm{M},k}$ decreases and so does the influence of the stabilization terms. Consequently, a limit is reached at which insufficient pressure stabilization occurs and zero pressure modes begin to spoil the solution. However, such pressure modes are highly mesh dependent and thus only observed for the distortion mode 3 where all elements exhibit the same distortion. In practical situations this will rarely be the case. Nevertheless, these results confirm that SUPG or GLS simulations are somewhat preferable compared with USFEM, which may require a determination of m_k within every time step when the mesh is moving.

4.4. Flow past cylinder

Incompressible flow past a rigid cylinder at a Reynolds number of $Re=100$ is a classical test case and has been investigated with respect to linear elements of high aspect ratio by Mittal [6]. We repeat parts of the computations reported in [6] and compare the behaviour of linear and quadratic elements.

The geometry and the mesh data used are depicted in Figure 9. Three different meshes of linear Q1Q1 elements are employed differing only in the region close to the cylinder, which is marked in light grey in Figure 9 where the number of elements along the edge of a subdivision of the domain is also given. The number of elements along the diagonal line a is 36, 48 and 90, yielding

DOI: 10.1002/fld

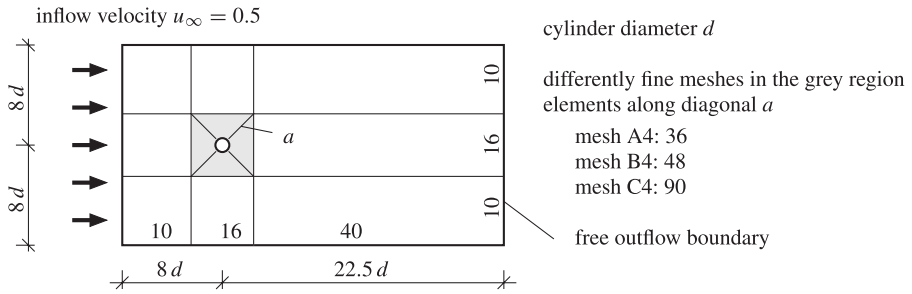

Figure 9. Flow past cylinder, geometry and mesh data.

a total number of elements of 4424, 5192 and 7880 for the meshes A4, B4 and C4, respectively. The elements along a are concentrated towards the cylinder such that a maximal aspect ratio of the order of magnitude of 10^1, 10^3 and 10^5 results for the three respective meshes A4, B4 and C4. A second set of three meshes A9, B9 and C9 of quadratic Q2Q2 elements is defined in the same way by taking half the number of elements at every edge yielding in total a quarter of the respective linear elements.

The fluid has a viscosity of $\nu = 0.005$, a density of $\rho = 1.0$ and an inflow velocity of $u_\infty = 0.5$ is prescribed. At the top and bottom boundary the flow is allowed to slip frictionless along the wall. Following Mittal in all cases a time step of $\Delta t = 0.125$ has been used.

The parameters used within the stabilization operator are $\eta = 0.0$, $\alpha = -1.0$ and $\beta = -1.0$. Thus, stabilization is employed in its best-natured formulation, which is not the SUPG type of stabilization that was used by Mittal in [6]. A further difference might stem from slightly different time discretization schemes. Thus, the results cannot be expected to be perfectly identical to those obtained by Mittal.

We compare the performance of the approach used with the element length definitions given in point (i), (vi) and (vii) of Section 3.2, i.e. a length definition based on the square root of the elemental area and the minimal and maximal element lengths $h_{k,\min}$ and $h_{k,\max}$ on the three meshes.

Figures 10–12 display the temporal evolution of the lift and drag coefficients

$$C_\mathrm{l} = \frac{2F_\mathrm{l}}{\rho u_\infty \mathrm{d}} \quad \text{and} \quad C_\mathrm{d} = \frac{2F_\mathrm{d}}{\rho u_\infty \mathrm{d}}$$

in selected cases, where F_l and F_d denote the lift and drag force, respectively. Additionally, the normalized pressure distribution along the cylinder obtained from

$$C_p(x) = \frac{2(p(x) - p_0)}{\rho u_\infty^2} + 1$$

where p_0 denotes the pressure at the stagnation point of the cylinder, is given in Figure 10 for the mesh A4 and again in Figure 13 for mesh C9 and the minimal element length according to (vi). The respective diagrams for all other cases are very similar and thus omitted. Following Mittal in [6], the pressure distribution is projected to the horizontal direction. The pressure distribution is evaluated at a maximum of the lift coefficient.

DOI: 10.1002/fld

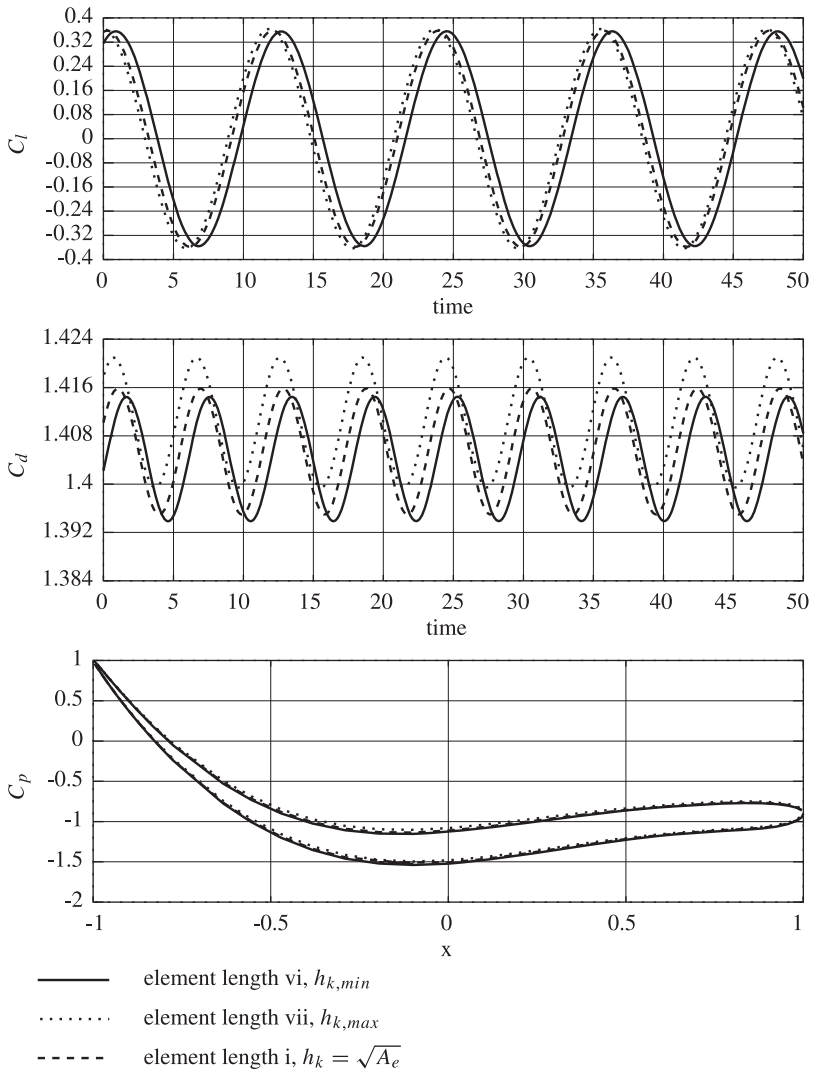

Figure 10. Lift and drag forces obtained on mesh A4 with three different element length definitions within the stabilization parameter.

In Figure 10, which shows the behaviour of the linear Q1Q1 elements, a slight dependency of the results on the stabilization parameter definition can be seen. In particular, the lift value shows a deviation when $h_{k,\max}$ is employed. This is due to the increasing influence of the inconsistency of linear elements. In contrast to the results reported by Mittal [6], who for some stabilization parameter definitions observed oscillations on the mesh with the highest aspect ratio, we do not detect increasing differences or instabilities when the aspect ratio is increased up to the order of magnitude of 10^5.

The results obtained from linear elements on the three different meshes are compared in Figure 11. Even the pressure profile along the cylinder remains correct up to the most distorted

DOI: 10.1002/fld

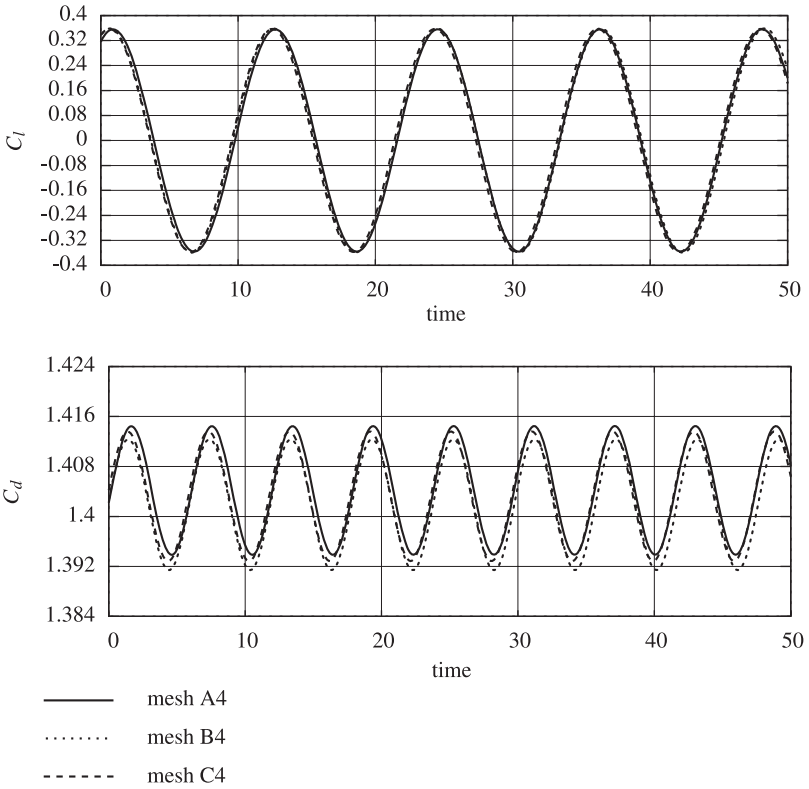

Figure 11. Lift and drag coefficients obtained on linear meshes with minimal element length according to (vi).

mesh used. This difference might possibly be influenced by the fact that in contrast to Mittal not an SUPG type of stabilization, but rather GLS has been used here.

The results obtained with quadratic Q2Q2 elements are even better. In Figure 12, the resulting lift and drag coefficients on the quadratic meshes are shown, which exhibit very similar and stable behaviour. The horizontal offset of these curves is caused by different initial dynamics during the inflow phase. The actual onset of the vortex shedding is very sensitive to the actual amount of diffusion but also to numerical parameters such as slightly unsymmetric meshes. As soon as the final vortex shedding has developed, very similar characteristics are obtained. With the quadratic elements and the element length definition $h_{k,\min}$, the pressure distribution yields a tiny disposition to oscillations between the edge and corner nodes of the elements. This oscillation can be observed in the zoom in Figure 13, where the diagram obtained on the mesh C9 is shown. Very similar results have been obtained on the other two quadratic meshes. This effect indicates that $h_{k,\min}$ marks a lower bound for the element length in highly distorted elements with respect to the necessary pressure stabilization.

Although still offering very good results, highly stretched elements yield badly conditioned matrices and thus the solution may require particular consideration. We used the iterative solver package 'Aztec' with a GMRES solver for the meshes A4, B4, C4 and A9, which failed to converge

DOI: 10.1002/fld

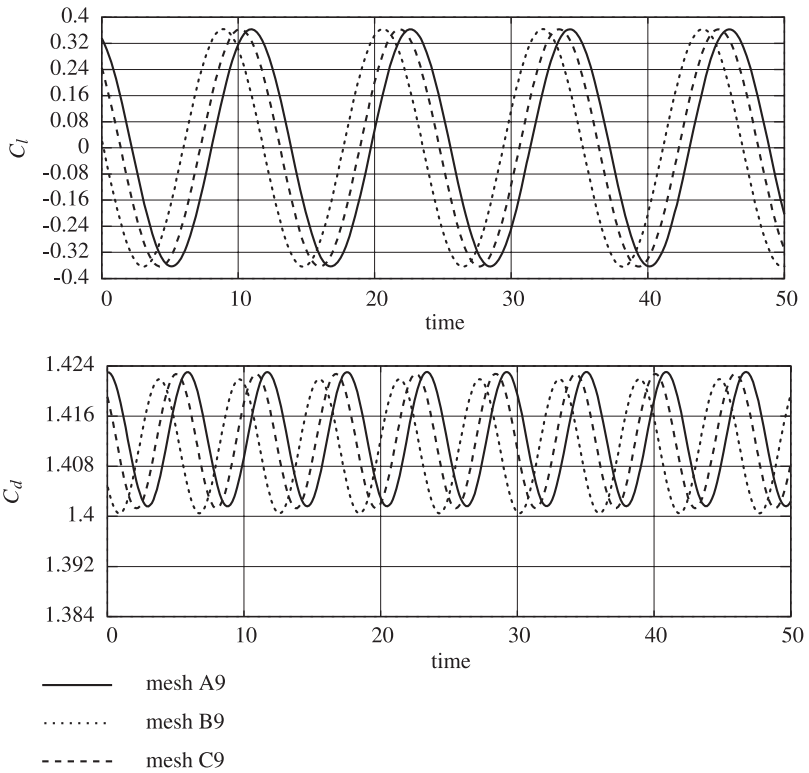

Figure 12. Lift and drag coefficients obtained on quadratic meshes with element length according to (i).

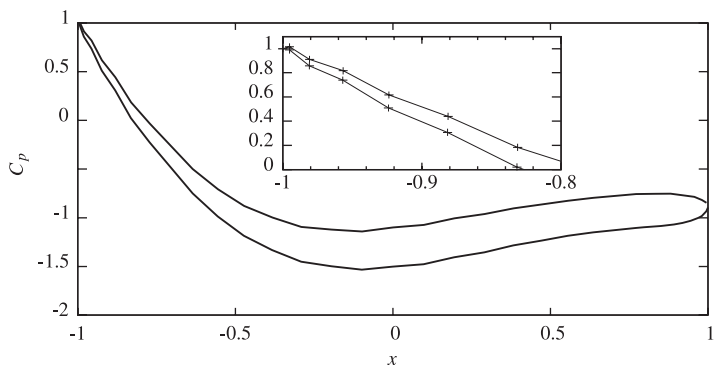

Figure 13. Slightly oscillating pressure profile with close-up view obtained on Mesh C9 with minimal element length (vi).

for the remaining cases B9 and C9. There a direct solver had to be employed. However, as the condition problem is related to single nodes or degrees of freedom of highly stretched elements, appropriate scaling could be introduced removing the problem if these elements have to be used.

DOI: 10.1002/fld

Table VI. Strouhal number in the different cases.

Mesh	Number of elements	Number of nodes	Aspect ratio	Element length (vi) Strouhal number	Element length (vii) Strouhal number	Element length (i) Strouhal number
A4	4424	4558	10	0.16949	0.16878	0.16913
B4	5192	5326	10^3	0.16807	0.16701	0.16736
C4	7880	8014	10^5	0.16878	0.16807	0.16842
A9	1106	4558	10	0.17131	0.17131	0.17167
B9	1298	5326	10^3	0.17094	0.17058	0.17058
C9	1970	8014	10^5	0.17131	0.17131	0.17131

Table VI gives an overview over the Strouhal numbers $St = d/(Tu_\infty)$ obtained on the different meshes with the different stabilization parameter definitions. The maximal and minimal obtained Strouhal numbers differ by less than 3%, which is just half the variation obtained by Mittal on the Q1Q1 mesh [6].

It is further observed that quadratic elements in all cases yield a slightly higher Strouhal number indicating that even for the very fine meshes employed around the cylinder quadratic elements are able to offer more accurate results. In addition, the mean value of the drag coefficient on the cylinder obtained with quadratic elements is higher than when linear elements are used. This is due to the lower numerical damping introduced by the stabilization terms in the case of quadratic elements.

Mittal concludes that the element length $h_{k,\min}$ works best. Nevertheless, he reported some pressure oscillations in the vicinity of the cylinder when this element length was used. As he used linear elements at $Re = 100$, these conclusions are in perfect accordance with our findings. Higher stabilization caused by a higher element length may well introduce a significant amount of artificial diffusion due to badly resolved second-order terms within the stabilization terms. Consequently, linear elements perform better for lower stabilization parameters. However, there is a lower bound for the stabilization parameter as artificial pressure modes need to be stabilized as well. Consequently, local pressure oscillations might well be observed when very low stabilization is employed.

5. SUMMARY AND CONCLUSIONS

Stabilized finite element methods for incompressible flow can well be used on distorted meshes and are thus applicable for ALE formulations. Nevertheless, some care should be taken in order to maximize the accuracy of the results in particular to deforming meshes. It is generally advisable to employ a GLS or SUPG type of the method rather than a correct USFEM if the constant m_k is not determined exactly.

Only minor differences between different definitions of the element length have been obtained, which indicates that the element length definition is not crucial in many cases. Thus, a purely geometric definition of the element length such as the square root of the element area is well applicable in particular as this choice does not add to the nonlinearity of the problem. However, on heavily stretched or skewed elements, the maximal element length definition may yield significant over-stabilization, which introduces high errors. This is particularly critical when linear elements

DOI: 10.1002/fld

are employed, which exhibit an inconsistency error which scales with the amount of stabilization. Thus, higher-order elements are advisable for computations by means of residual-based stabilized finite elements on distorted meshes.

The numerical investigation of flow around a cylinder at Reynolds number 100 with Q1Q1 elements reported by Mittal [6] has been repeated, while the results obtained here do not exhibit any unphysical oscillations on meshes with a maximal aspect ratio up to an order of 10^5. We further extended the numerical investigation to biquadratic elements for comparison. In particular, when quadratic Q2Q2 elements are employed all the definitions considered for the stabilization parameter, i.e. for the characteristic element length yield almost identical results. Even on these fine meshes a small difference in the Strouhal number obtained with linear or quadratic elements can be found, indicating that the superior accuracy of quadratic elements is significant even on very fine meshes. This finding is also stressed by the fact that the mean value of the drag coefficient is higher when quadratic elements are employed.

It was further found that in a variety of test cases SUPG performed better than GLS. The difference is particularly remarkable for linear elements but also on meshes of quadratic elements with offset edge nodes the effect occurs. The reason is to be found in the viscous term, which contains second derivatives that are approximated worst compared with lower-order terms. Thus, dropping the second derivatives from the stabilization operator improves the accuracy on distorted meshes.

The superiority of quadratic elements is based on a regular placement of the element edge and centre nodes. Small displacements of edge nodes perpendicular to the original edge still maintains the good performance of the element, while highly offset edge nodes significantly increase the error. In practical applications, a good geometry approximation can be obtained by placing the edge node with an offset of up to a quarter of the element length.

ACKNOWLEDGEMENTS

The present study is supported by a grant of the foundation 'Deutsche Forschungsgemeinschaft' (DFG) under project B4 of the collaborative research centre SFB 404 'Multield Problems in Continuum Mechanics'. This support is gratefully acknowledged.

REFERENCES

1. Tezduyar TE, Osawa Y. Finite element stabilization parameters computed from element matrices and vectors. *Computer Methods in Applied Mechanics and Engineering* 2000; **190**:411–430.
2. Akin JE, Tezduyar TE. Calculation of the advective limit of the SUPG stabilization parameter for linear and higher order elements. *Computer Methods in Applied Mechanics and Engineering* 2004; **193**:1909–1922.
3. Codina R, Soto O. Approximation of the incompressible Navier–Stokes equations using orthogonal subscale stabilization and pressure segregation on anisotropic finite element meshes. *Computer Methods in Applied Mechanics and Engineering* 2004; **193**:1403–1419.
4. Taylor CA, Hughes TJR, Zarins CK. Finite element modeling of blood flow in arteries. *Computer Methods in Applied Mechanics and Engineering* 1998; **158**:155–196.
5. Whiting CH, Jansen KE. A stabilized finite element method for the incompressible Navier–Stokes equations using a hierarchical basis. *International Journal for Numerical Methods in Fluids* 2001; **35**:93–116.
6. Mittal S. On the performance of high aspect ratio elements for incompressible flows. *Computer Methods in Applied Mechanics and Engineering* 2000; **188**:269–287.
7. Harari I. Spatial stability of semidiscrete formulations for parabolic problems. *Proceedings of the Fifth World Congress on Computational Mechanics 2002*, Vienna, Austria, 2002.

DOI: 10.1002/fld

8. Barth T, Bochev PB, Gunzburger MD, Shadid JN. A taxonomy of consistently stabilized finite element methods for the Stokes problem. *SIAM Journal on Scientific Computing* 2004; **25**:1585–1607.
9. Franca LP, Hughes TJR. Two classes of mixed finite element methods. *Computer Methods in Applied Mechanics and Engineering* 1988; **69**:89–129.
10. Behr M. Stabilized finite element methods for incompressible flows with emphasis on moving boundaries and interfaces. *Ph.D. Thesis*, Faculty of the Graduate School of the University of Minnesota, 1992.
11. Wall WA. Fluid–Struktur-Interaktion mit stabilisierten Finiten Elementen. *Ph.D. Thesis*, Institute of Structural Mechanics, Universität Stuttgart, 1999.
12. Franca LP, Oliveira SP. Pressure bubbles stabilization features in the Stokes problem. *Computer Methods in Applied Mechanics and Engineering* 2003; **192**:1929–1937.
13. Franca LP, Farhat C. Bubble functions prompt unusual stabilized finite element methods. *Computer Methods in Applied Mechanics and Engineering* 1995; **123**:299–308.
14. Franca LP, Farhat C, Lesoinne M, Russo A. Unusual stabilized finite element methods and residual free bubbles. *International Journal for Numerical Methods in Fluids* 1998; **27**:159–168.
15. Franca LP, Valentin F. On an improved unusual stabilized finite element method for the advective–reactive–diffusive equation. *Computer Methods in Applied Mechanics and Engineering* 2000; **190**:1785–1800.
16. Förster Ch. Robust methods for fluid–structure interaction with stabilized finite elements. *Ph.D. Thesis*, Institute of Structural Mechanics, Universität Stuttgart, 2007.
17. Barrenechea GR, Valentin F. An unusual stabilized finite element method for a generalized Stokes problem. *Numerische Mathematik* 2002; **92**:652–677.
18. Harari I, Hughes TJR. What are C and h?: inequalities for the analysis and design of finite element methods. *Computer Methods in Applied Mechanics and Engineering* 1992; **97**:157–192.
19. Jansen EK, Collis SS, Whiting C, Shakib F. A better consistency for low-order stabilized finite element methods. *Computer Methods in Applied Mechanics and Engineering* 1999; **174**:153–170.
20. Whiting CH. Stabilized finite element methods for fluid dynamics using a hierarchical basis. *Ph.D. Thesis*, Rensselaer Polytechnic Institute, 1999.
21. Tezduyar TE. Computation of moving boundaries and interfaces and stabilization parameters. *International Journal for Numerical Methods in Fluids* 2003; **43**:555–575.
22. Tezduyar TE, Park YJ. Discontinuity-capturing finite element formulations for nonlinear convection–diffusion–reaction equations. *Computer Methods in Applied Mechanics and Engineering* 1986; **59**:307–325.
23. Douglas J, Wang J. An absolutely stabilized finite element method for the Stokes problem. *Mathematics of Computation* 1989; **52**:495–508.
24. Franca LP, Madureira AL. Element diameter free stability parameters for stabilized methods applied to fluids. *Computer Methods in Applied Mechanics and Engineering* 1993; **105**:395–403.

DOI: 10.1002/fld